Rooftop optical modulation stabilizes urban photovoltaics across seasons

Samiran Khorat[1], Ansar Khan[2*], Rupali Khatun[1], Debashish Das[3], Thanh-Hung Nguyen[4], Konstantina Vasilakopoulou[5], Deepak Amaripadath[6], Lidia Vitanova[7], Rafiq Hamdi[8,9], Dev Niyogi[10,11], Mattheos Santamouris[12]

[1]School of Environmental Studies, Jadavpur University, Kolkata, India
[2]Department of Geography, Lalbaba College, University of Calcutta, Kolkata, India
[3]Department of Architecture, Jadavpur University, Kolkata, India
[4]Tropical Marine Science Institute, National University of Singapore, Singapore, Singapore
[5]School of Property, Construction and Project Management, Royal Melbourne Institute of Technology, Melbourne, Australia
[6]School of Geographical Sciences and Urban Planning, Arizona State University, Tempe, United States
[7]GATE Institute – Big Data for Smart Society, Sofia University, Sofia, Bulgaria
[8]Royal Meteorological Institute of Belgium, Brussels, Belgium
[9]State Key Laboratory of Desert and Oasis Ecology, Xinjiang Institute of Ecology and Geography, Chinese Academy of Sciences, Beijing, China
[10]Department of Earth and Planetary Sciences, Jackson School of Geosciences, University of Texas at Austin, Austin, United States
[11]Maseeh Department of Civil, Architectural, and Environmental Engineering, Cockrell School of Engineering, University of Texas at Austin, Austin, United States
[12]School of Built Environment, University of New South Wales, Sydney, Australia

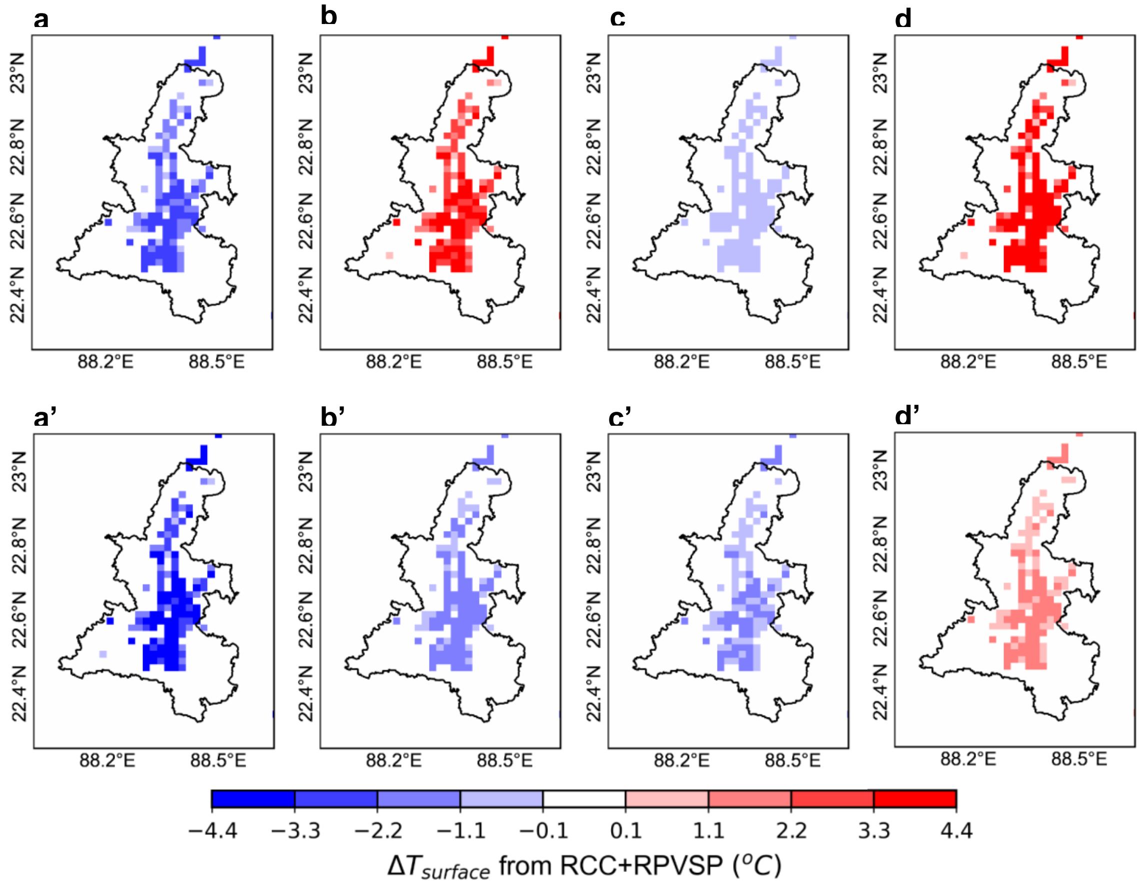

Fig. S1 | Spatial response of changes (scenario minus RCC+RPVSP) in simulated surface temperature to rooftop PDRC configurations integrated with RPVSPs during summer over Kolkata.

Panel (a-d) shows daytime and (a′-d′) nighttime changes in surface temperature ($\Delta T_{\mathrm{surface}}$) relative to the RCC+RPVSP configuration, averaged over urban grid cells within the Kolkata urban region (denoted by black line inside the box). Panels correspond to different rooftop PDRC configurations integrated with RPVSPs: (a, a’) nm-PDRC+RPVSP; (b, b’) ρ-PDRC+RPVSP; (c, c’) ε-PDRC+RPVSP; and (d, d) ρε-PDRC+RPVSP. The RCC+RPVSP configuration represents conventional reinforced cement concrete rooftops integrated with RPVSPs**.**

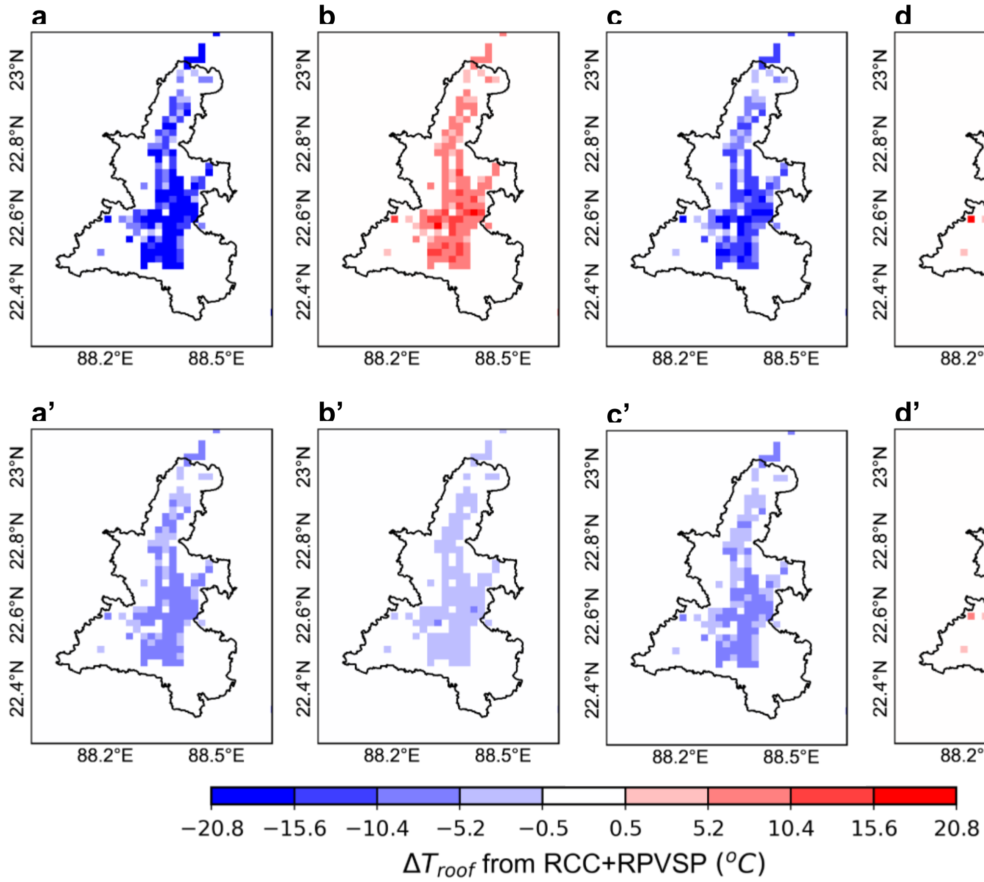

Fig. S2 | Same as Fig. S1, but for roof surface temperature (ΔT_{roof})

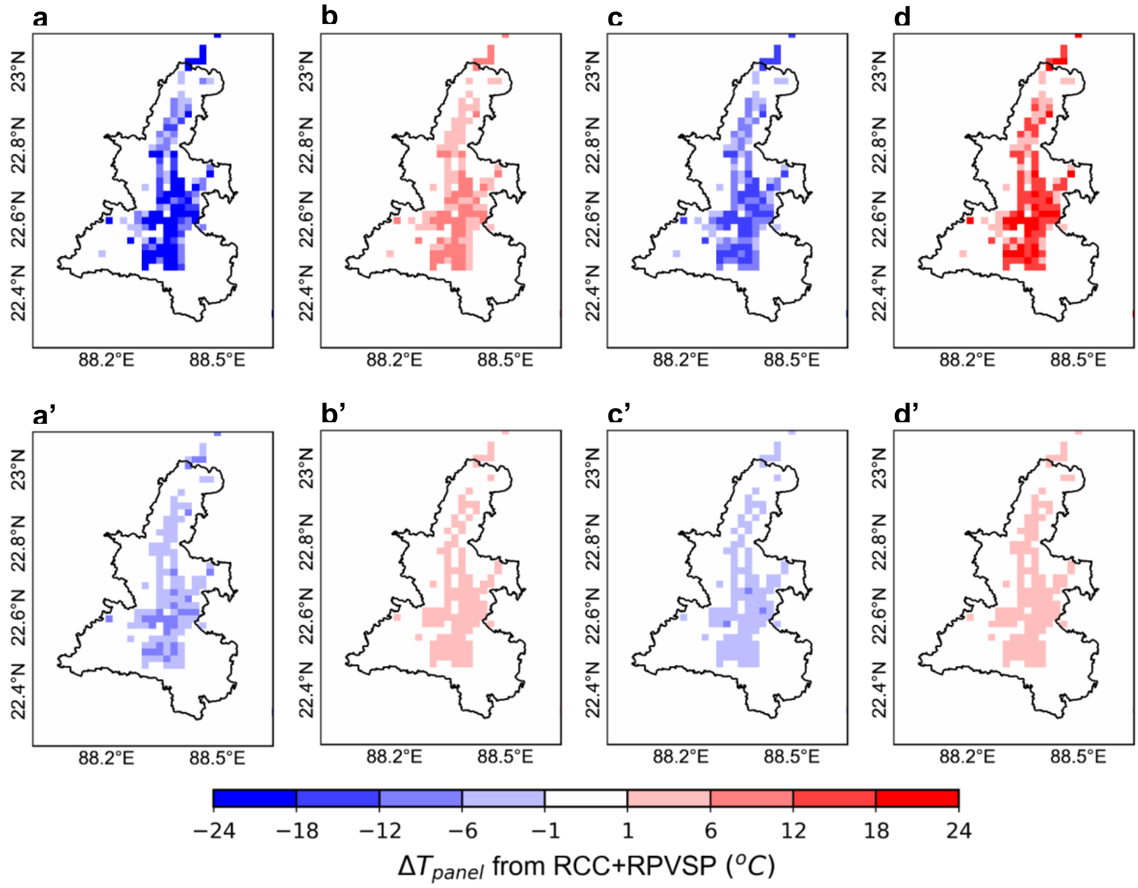

Fig. S3 | Same as Fig. S1, but for panel surface temperature (ΔT_{panel})

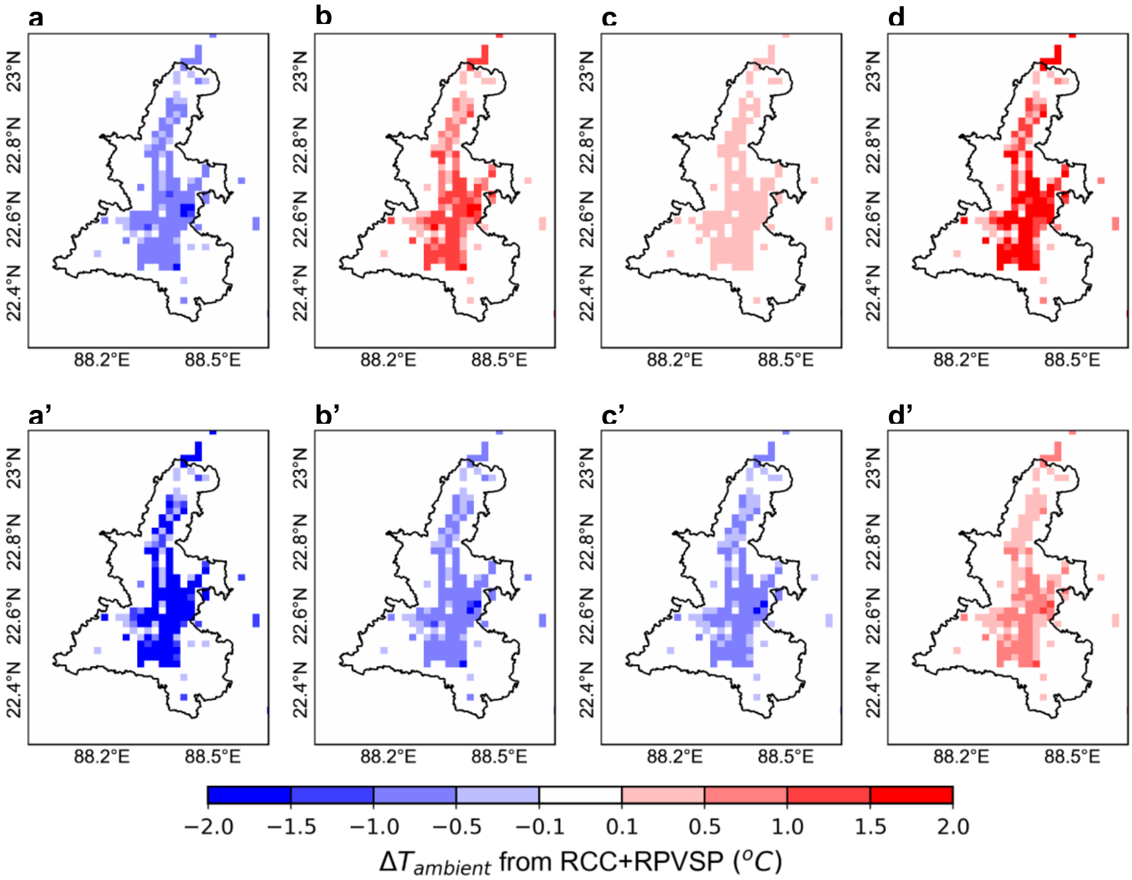

Fig. S4 | Spatial response of changes (scenario minus RCC+RPVSP) in simulated ambient temperature to rooftop PDRC configurations integrated with RPVSPs during winter over Kolkata. Panel (a-d) shows daytime and (a′-d′) nighttime changes in ambient temperature ($\Delta T_{\mathrm{ambient}}$) relative to the RCC+RPVSP configuration, averaged over urban grid cells within the Kolkata urban region (denoted by black line inside the box). Panels correspond to different rooftop PDRC configurations integrated with RPVSPs: (a, a’) nm-PDRC+RPVSP; (b, b’) ρ-PDRC+RPVSP; (c, c’) ε-PDRC+RPVSP; and (d, d) ρε-PDRC+RPVSP. The RCC+RPVSP configuration represents conventional reinforced cement concrete rooftops integrated with RPVSPs**.**

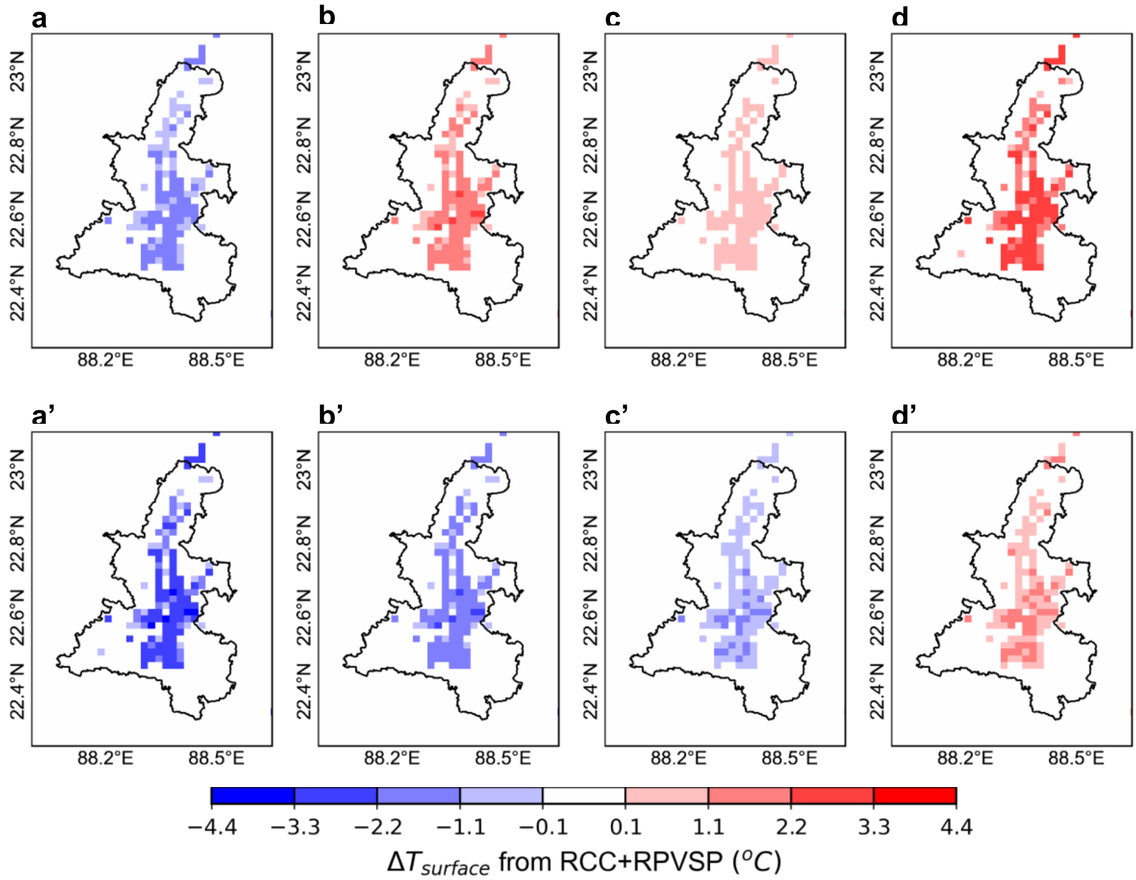

Fig. S5 | Same as Fig. S4, but for surface temperature ($\Delta T_{\mathrm{surface}}$)

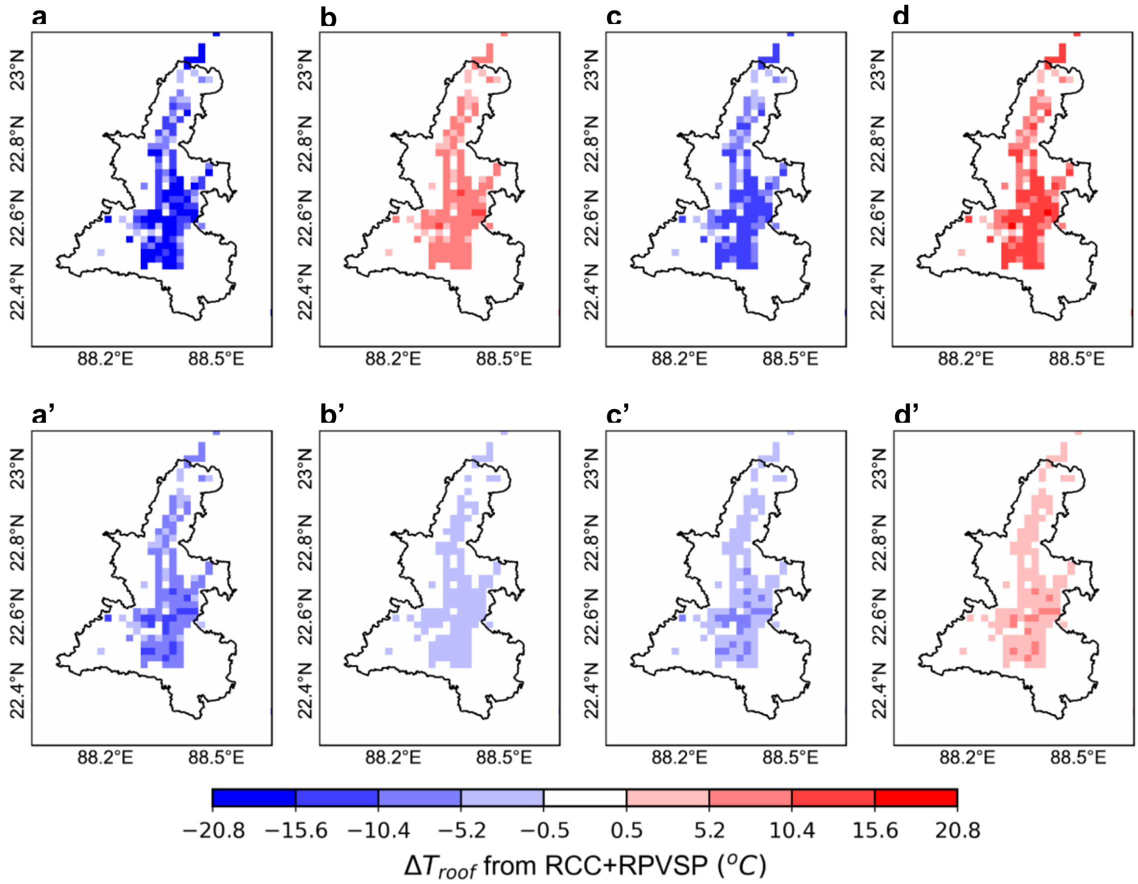

Fig. S6 | Same as Fig. S4, but for roof surface temperature (ΔT_{roof})

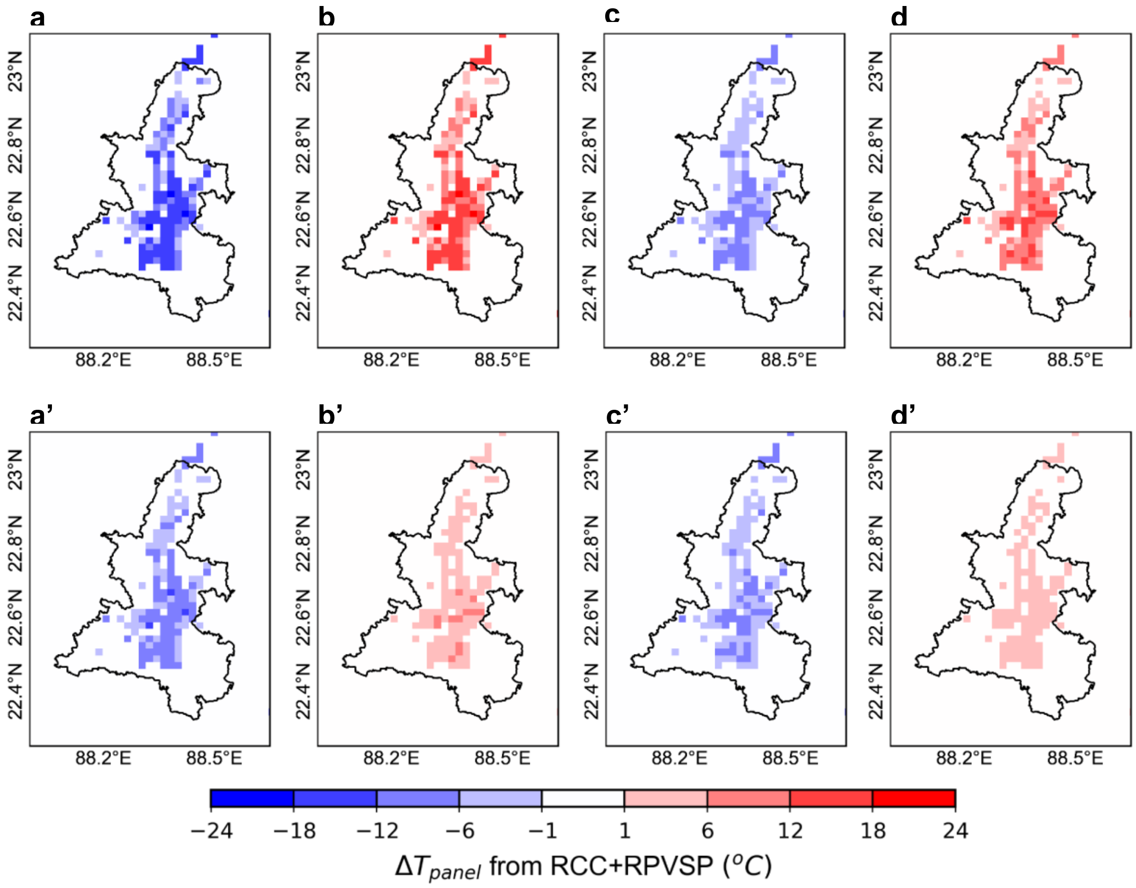

Fig. S7 | Same as Fig. S4, but for panel surface temperature (ΔT_{panel})

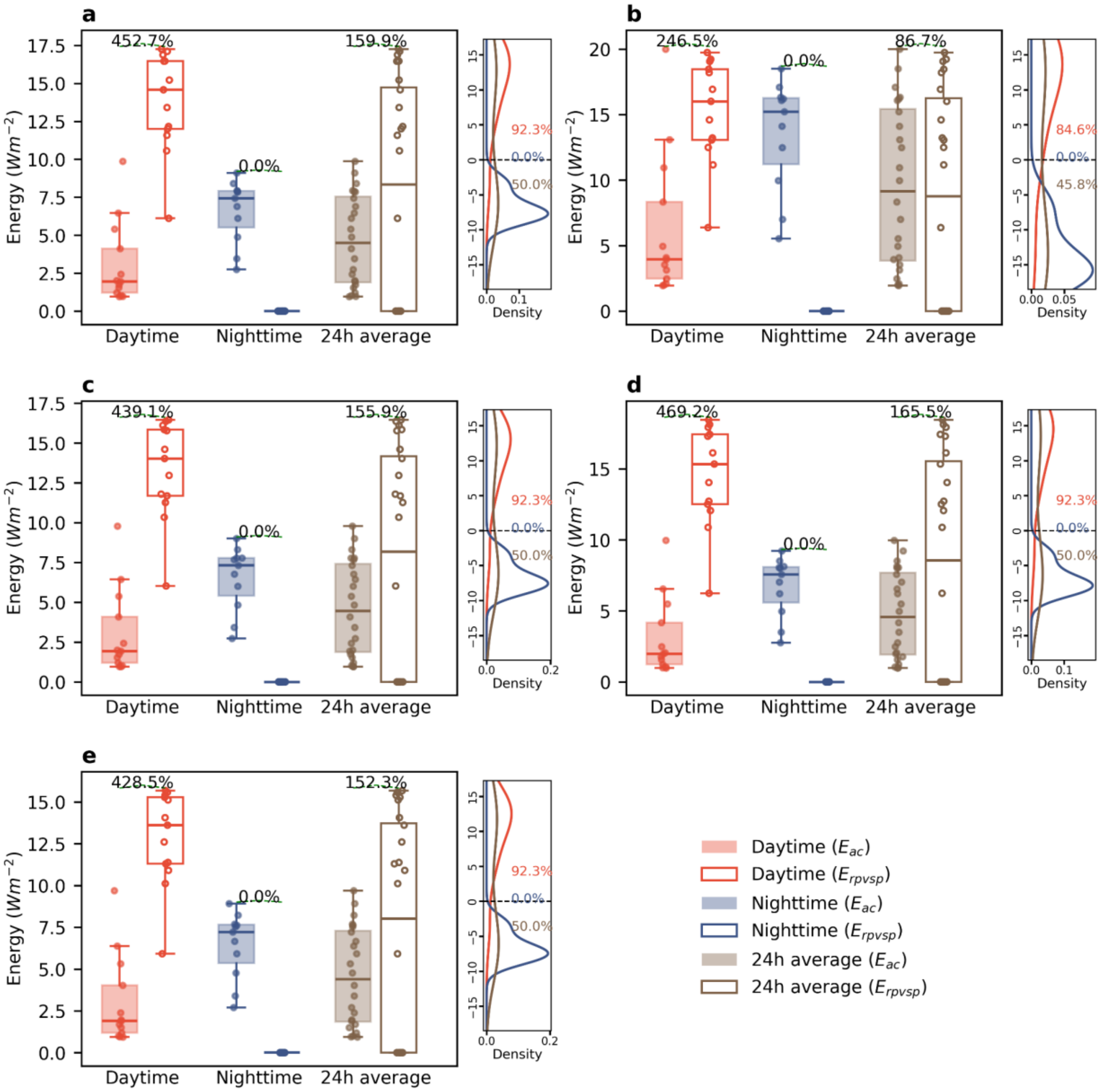

Fig. S8 | Distribution of building AC-energy demand and RPVSP energy generation under RPVSP-integrated PDRC roofing configurations during winter.

Box-scatter distributions compare urban-grid-cell-averaged building air-conditioning (AC) energy demand (E_{ac}) and RPVSP energy generation (E_{rpvsp}) during daytime, nighttime and 24 h average conditions across the Kolkata metropolitan region under different RPVSP-integrated roofing configurations: a, baseline scenario (RCC+RPVSP); b, nm-PDRC+RPVSP; c, ρ-PDRC+RPVSP; d, ε-PDRC+RPVSP; and e, ρε-PDRC+RPVSP. Percentage values above each pair denote the fraction of building AC-energy demand offset by RPVSP energy generation under each roofing configuration. Inset panels show kernel density estimates of net energy balance (RPVSP-AC energy demand) across urban grid cells, with vertical orientation to emphasize distribution spread and skewness. The dashed horizontal line marks zero balance, separating surplus (positive) from deficit (negative) conditions. Annotated percentages within insets indicate the probability of surplus occurrence for each time period, color-coded consistently with the main panels.

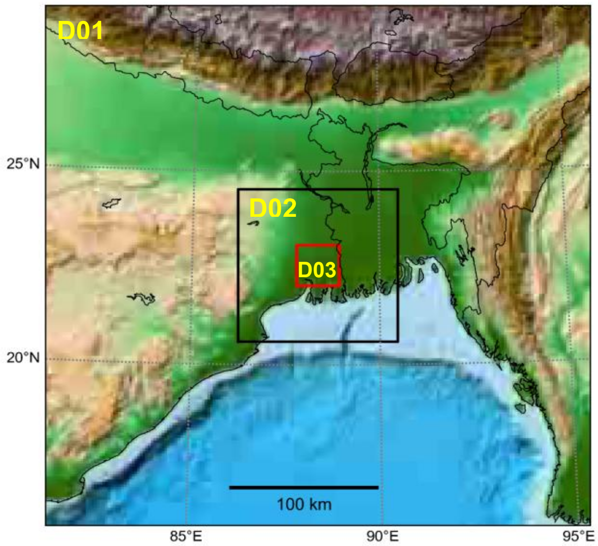

Fig. S9 | Nested Weather Research and Forecasting (WRF v4.7.0) model domains used for the city-scale simulations over the Kolkata metropolitan region.

The modelling framework employed a one-way nested dynamic downscaling configuration, consisting of the outermost parent domain (d01) with an 18 km horizontal grid spacing, an intermediate domain (d02) with a 6 km grid spacing, and the innermost urban-scale domain (d03) centred over the Kolkata urban region with a 2 km grid spacing. The nested configuration was designed to resolve large-scale synoptic forcing, regional mesoscale atmospheric processes, and fine-scale urban meteorological variability associated with land-atmosphere interactions across the Kolkata urban area.

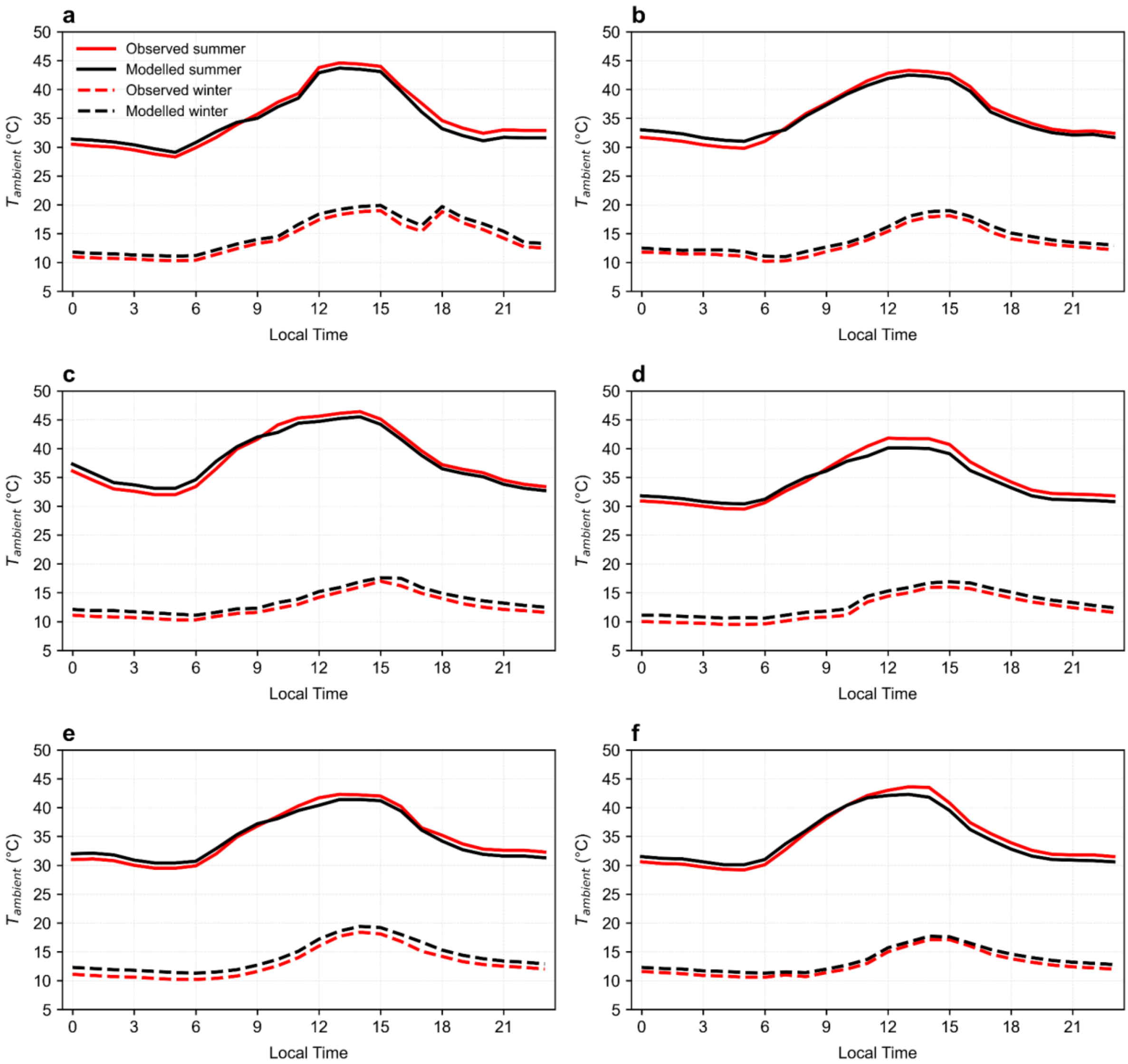

Fig. S10 | Validation of simulated (WRF-urban scheme) near-surface air temperature against station observations during summer and winter across the Kolkata metropolitan region.

Hourly variations of observed and modelled 2-m air temperature ($T_{ambient}$) at six observational stations: a) Ballygunge, b) BelurMath, c) Bidhan Nagar, d) Jadavpur, e) Rabindra Bharati University, and f) Rabindra Sarobar during summer and winter. The modelling framework successfully reproduced the diurnal evolution of near-surface air temperature across different urban environments in both seasons.

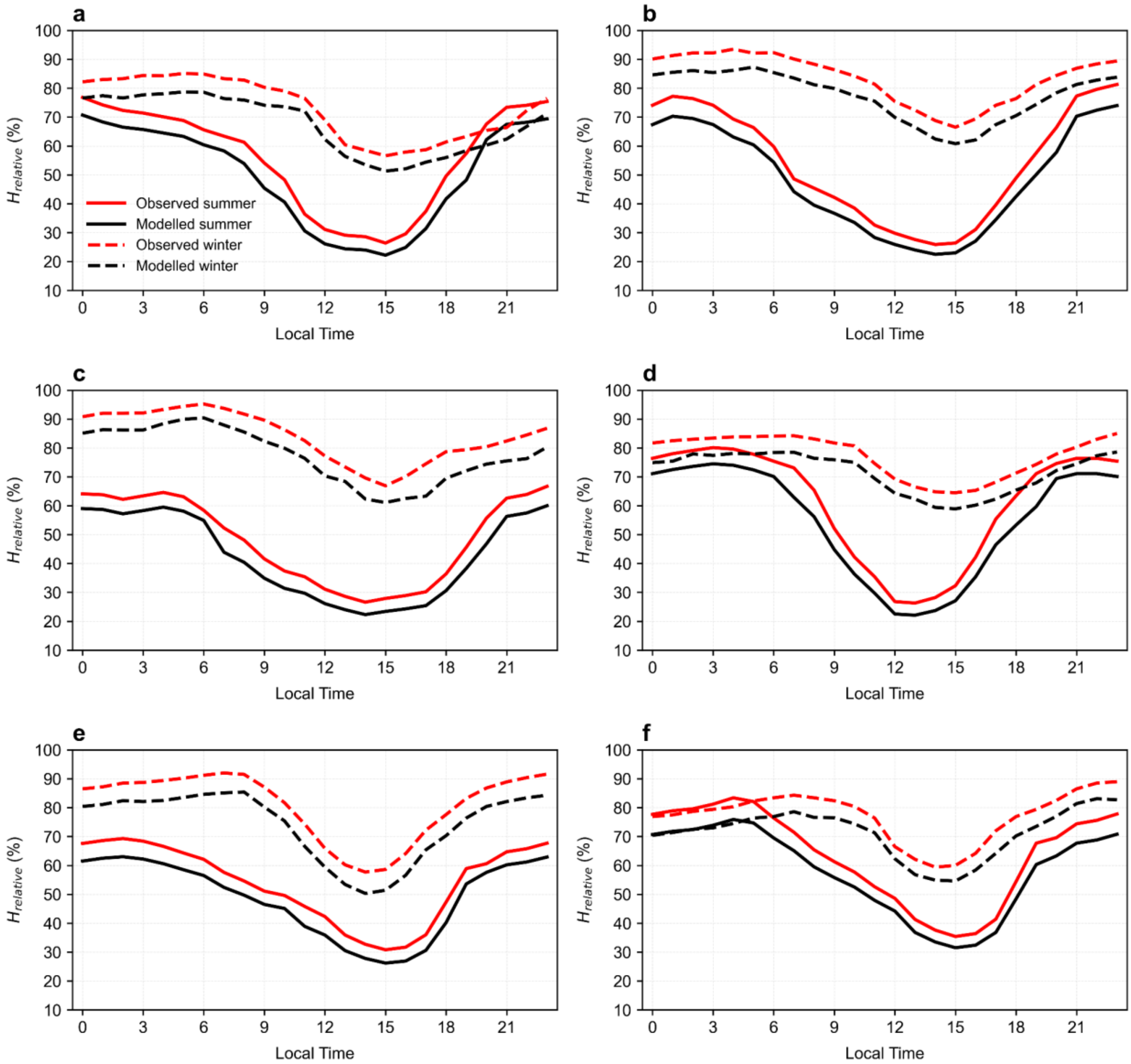

Fig. S11. | Same as Figure S10, but for Relative humidity ($H_{relative}$).

Table S1 | Seasonal changes in near-surface air temperature ($\Delta T_{ambient,}$ °C) induced by different optically modulated PDRC rooftop configurations integrated with RPVSPs across the Kolkata urban region. Changes are calculated relative to the baseline RCC+RPVSP configuration (scenario minus RCC+RPVSP) and spatially averaged over urban grid cells during summer and winter periods.

Seasons	Parameters / Scenarios	Maximum (daytime)	Maximum (nighttime)	Daytime average	Nighttime average	Daily average
Summer	nm-PDRC+RPVSP	-1.0	-1.5	-0.7	-1.0	-0.8
	ρ-PDRC+RPVSP	1.6	-0.8	1.1	-0.5	0.4
	ε-PDRC+RPVSP	-0.2	-0.3	-0.2	-0.2	-0.2
	ρε-PDRC+RPVSP	1.9	0.9	1.4	0.6	1.0
Winter	nm-PDRC+RPVSP	-0.9	-1.7	-0.6	-1.2	-0.9
	ρ-PDRC+RPVSP	1.4	-0.9	1.0	-0.5	0.3
	ε-PDRC+RPVSP	0.1	-0.9	0.2	-0.6	-0.2
	ρε-PDRC+RPVSP	1.7	0.8	1.2	0.6	0.9

Table S2 | Seasonal changes in surface temperature ($\Delta T_{surfacet}$), °C induced by different optically modulated PDRC rooftop configurations integrated with RPVSPs across the Kolkata urban region. Changes are calculated relative to the baseline RCC+RPVSP configuration (scenario minus RCC+RPVSP) and spatially averaged over urban grid cells during summer and winter periods.

Seasons	Scenarios \ Parameter	Maximum (daytime)	Maximum (nighttime)	Daytime average	Nighttime average	Daily average
Summer	nm-PDRC+RPVSP	-2.2	-3.9	-1.4	-2.7	-2.0
	ρ-PDRC+RPVSP	3.4	-1.5	2.5	-1.2	0.8
	ε-PDRC+RPVSP	-0.5	-1.0	-0.3	-0.6	-0.5
	ρε-PDRC+RPVSP	4.1	1.4	2.7	1.0	1.9
Winter	nm-PDRC+RPVSP	-1.2	-2.3	-0.8	-1.6	-1.1
	ρ-PDRC+RPVSP	2.1	-1.6	1.5	-1.0	0.3
	ε-PDRC+RPVSP	0.1	-0.7	0.2	-0.5	-0.1
	ρε-PDRC+RPVSP	3.1	1.0	2.1	0.7	1.4

Table S3 | Seasonal changes in roof surface temperature ($\Delta T_{roof,}$ °C) induced by different optically modulated PDRC rooftop configurations integrated with RPVSPs across the Kolkata urban region. Changes are calculated relative to the baseline RCC+RPVSP configuration (scenario minus RCC+RPVSP) and spatially averaged over urban grid cells during summer and winter periods.

Seasons	Scenarios \ Parameter	Maximum (daytime)	Maximum (nighttime)	Daytime average	Nighttime average	Daily average
Summer	nm-PDRC+RPVSP	-20.1	-7.9	-13.5	-5.3	-9.7
	ρ-PDRC+RPVSP	6.2	-1.9	4.2	-1.4	1.6
	ε-PDRC+RPVSP	-16.2	-6.8	-10.9	-4.5	-8.0
	ρε-PDRC+RPVSP	16.9	3.0	11.3	2.0	7.0
Winter	nm-PDRC+RPVSP	-16.5	-10.1	-11.0	-6.7	-9.1
	ρ-PDRC+RPVSP	4.8	-1.6	3.3	-0.7	1.4
	ε-PDRC+RPVSP	-12.9	-5.2	-8.6	-3.5	-6.3
	ρε-PDRC+RPVSP	13.5	2.8	9.1	1.9	5.8

Table S4 | Seasonal changes in panel surface temperature (ΔT_{panel}, °C) induced by different optically modulated PDRC rooftop configurations integrated with RPVSPs across the Kolkata urban region. Changes are calculated relative to the baseline RCC+RPVSP configuration (scenario minus RCC+RPVSP) and spatially averaged over urban grid cells during summer and winter periods.

Seasons	Parameters / Scenarios	Maximum (daytime)	Maximum (nighttime)	Daytime average	Nighttime average	Daily average
Summer	nm-PDRC+RPVSP	-23.7	-11.5	-15.9	-8.6	-12.6
	ρ-PDRC+RPVSP	8.5	3.4	6.8	2.8	5.0
	ε-PDRC+RPVSP	-18.7	-8.9	-12.6	-6.7	-9.9
	ρε-PDRC+RPVSP	18.5	3.1	12.4	2.3	7.8
Winter	nm-PDRC+RPVSP	-19.5	-16.7	-13.1	-12.1	-12.6
	ρ-PDRC+RPVSP	17.9	5.9	14.4	6.9	11.0
	ε-PDRC+RPVSP	-15.2	-12.9	-10.2	-9.4	-9.8
	ρε-PDRC+RPVSP	12.5	3.0	8.4	2.2	5.5

Table S5. Seasonal impacts of different optically modulated PDRC rooftop configurations integrated with RPVSPs on net building energy consumption across the Kolkata urban region. Values represent relative changes in net building energy consumption (%) and corresponding absolute changes (within parentheses, Wm^{-2}) compared with the baseline RCC+RPVSP configuration (scenario minus RCC+RPVSP), spatially averaged over urban grid cells during summer and winter periods.

Seasons	Parameters / Scenarios	Maximum (daytime)	Maximum (nighttime)	Daytime average	Nighttime average	Daily average
Summer	nm-PDRC+RPVSP	-13.0(-3.0)	-21.3(-4.7)	-10.7(-2.3)	-14.1(-2.6)	-12.3(-2.5)
	ρ-PDRC+RPVSP	1.1(0.3)	2.1(0.5)	0.9(0.2)	1.4(0.3)	1.1(0.2)
	ε-PDRC+RPVSP	-3.1(-0.7)	-4.9(-1.1)	-2.5(-0.6)	-3.2(-0.6)	-2.8(-0.6)
	ρε-PDRC+RPVSP	5.6(1.3)	11.0(2.4)	4.6(1.0)	7.3(1.4)	5.8(1.2)
Winter	nm-PDRC+RPVSP	3.3(0.1)	5.4(0.4)	2.7(0.1)	3.6(0.3)	3.1(0.2)
	ρ-PDRC+RPVSP	-0.8(0.1)	-2.2(-0.2)	-0.6(-0.1)	-1.4(-0.1)	-1.0(-0.1)
	ε-PDRC+RPVSP	2.1(0.1)	2.5(0.2)	1.7(0.0)	1.7(0.1)	1.7(0.1)
	ρε-PDRC+RPVSP	-2.6(-0.1)	-4.1(-0.3)	-2.1(0.0)	-2.7(-0.2)	-2.4(-0.1)

Table S6 | Seasonal changes in RPVSP energy generation induced by different optically modulated PDRC rooftop configurations integrated with RPVSPs across the Kolkata urban region. Values represent percentage changes in RPVSP energy generation and corresponding absolute changes (within parentheses, Wm^{-2}) relative to the baseline RCC+RPVSP configuration (scenario minus RCC+RPVSP), spatially averaged over urban grid cells during summer and winter periods.

Seasons	Parameters / Scenarios	Maximum (daytime)	Maximum (nighttime)	Daytime average	Nighttime average	Daily average
Summer	nm-PDRC+RPVSP	12.3(2.8)	0	8.5(1.6)	0	4.6(10.6)
	ρ-PDRC+RPVSP	-3.7(-0.8)	0	-2.5(-0.5)	0	-1.4(-0.3)
	ε-PDRC+RPVSP	7.1(1.6)	0	4.9(0.9)	0	2.7(0.5)
	ρε-PDRC+RPVSP	-9.3(-2.1)	0	-6.4(-1.2)	0	-3.5(-0.7)
Winter	nm-PDRC+RPVSP	14.3(2.5)	0	9.8(1.4)	0	5.3(0.8)
	ρ-PDRC+RPVSP	-4.7(-0.8)	0	-3.4(-0.5)	0	-1.9(-0.3)
	ε-PDRC+RPVSP	6.9(1.2)	0	4.9(0.7)	0	2.7(0.4)
	ρε-PDRC+RPVSP	-9.7(-1.7)	0	-6.8(-1.0)	0	-3.7(-0.5)

Table S7 | Reported optical properties and sub-ambient cooling performance of PDRC materials from previous studies, and justification of the optical parameters adopted in the present city-scale RPVSP-integrated simulations. The table summarizes solar reflectance (ρ), thermal emittance (ε), reported sub-ambient temperature reductions, study type, and corresponding references for experimentally and numerically investigated PDRC materials. The selected optical properties used in the present study are positioned within the high-performance domain of previously reported radiative cooling materials

Sl no. (for Fig.8)	Structure and material	Solar reflectance (ρ)	Thermal emittance (ε)	Sub-ambient temperature drop (°C)	Study type	Ref.
1	SiO2 microspheres	0.96	0.94	12	Experiment	[1]
2	PVA-caprylic aldehyde	0.96	0.9	2.7	Experiment	[2]
3	SiO2-Si3N4-Al2O3-Ag	0.948	0.87	8.3	Experiment	[3]
4	acrylate + Al2O3+SiO2 particles	0.941	0.935	7.9	Experiment	[4]
5	Porous cellulose	0.9	0.9	15	Experiment	[5]
6	ZnO-SiO2	0.97	0.95	5.7	Experiment	[6]
7	Porous PEA	0.922	0.799	13	Experiment	[7]
8	Wood (cellulose)	0.96	0.9	9	Experiment	[8]
9	Aluminum phosphate (AlPO4)	0.97	0.9	4.2	Experiment	[9]
10	Acrylic + CaCO3 particles	0.955	0.94	1.7	Experiment	[10]
11	BaSO4 paints	0.976	0.96	4.5	Experiment	[11]
12	CA-PVA-CaCl2	0.95	0.94	10	Experiment	[12]
13	SiO2-SiOxN	0.964	0.946	2.5	Experiment	[13]
14	PDMS-P(VDF-HFP)	0.965	0.943	13.8	Experiment	[14]
15	BaSO4-ethyl cellulose	0.986	0.981	2.5	Experiment	[15]
16	Porous PVDF	0.96	0.97	6	Experiment	[16]
17	PDMS + glass bubbles	0.92	0.85	5.3	Experiment	[17]
18	PVDF-MXene dual mode	0.967	0.961	11.7	Experiment	[18]
19	SiO2-PVA metafiber	0.97	0.9	6	Experiment	[19]
20	Porous PVDF + SiO2 spheres	0.97	0.96	6	Simulation	[20]
21	PMMA	0.95	0.98	8.2	Experiment	[21]
22	Cellulose acetate-CsPbX3 quantum dots	0.9	0.95	5.6	Experiment	[22]
23	PTFE-POM	0.954	0.832	9	Experiment	[23]
24	Porous PCA?+?SiO2 spheres	0.96	0.95	6.2	Experiment	[24]
25	P(VdF-HFP)-Al2O	0.9826	0.9756	9.1	Experiment	[25]
26	PDMS+Al2O3 spheres	0.95	0.96	5.1	Experiment	[26]
27	PE-Ag	0.95	0.86	10.6	Experiment	[27]
28	Porous PDMS	0.93	0.94	5	Experiment	[28]
29	PTFE-Ag	0.98	0.86	2.7	Experiment	[29]
30	Cotton + PDMS-AlPO4	0.97	0.94	5.4	Experiment	[30]
31	Porous PE?+?SiO2 spheres	0.962	0.9	6.1	Experiment	[31]
32	SiO2-Si3N4-Al2O3-Ag	0.966	0.908	8.6	Simulation	[32]
33	Al2O	0.95	0.9	3.5	Experiment	[33]
Present Study	NM+PDRC	0.95	0.93			

Table S8 | Seasonal urban thermal and rooftop photovoltaic panel responses to PDRC-integrated roofing configurations across Delhi and Kuala Lumpur. Changes in ambient air temperature, urban surface temperature, roof surface temperature, and rooftop photovoltaic (RPVSP) panel temperature are summarized for summer and winter conditions relative to the baseline RCC+RPVSP configuration. Values represent spatially averaged differences across urban grid cells during both seasons. Negative values indicate cooling effects induced by the PDRC-integrated rooftop configuration compared with the baseline scenario.

Seasons	Parameters	Ambient Temp. (°C)		Surface Temp. (°C)		Roof surface Temp. (°C)		Panel Temp. (°C)	
		Delhi	Kuala Lumpur	Delhi	Kuala Lumpur	Delhi	Kuala Lumpur	Delhi	Kuala Lumpur
Summer	Maximum (daytime)	-1.3	-0.9	-2.6	-1.9	-23.1	-18.9	-25.5	-20.8
	Maximum (nighttime)	-1.7	-1.3	-4.2	-3.4	-9.5	-5.9	-15.1	-10.1
	Daytime average	-0.9	-0.5	-1.9	-1.2	-15.7	-11.2	-18.0	-13.4
	Nighttime average	-1.2	-0.8	-3.2	-2.3	-7.2	-3.8	-11.0	-7.0
	Daily average	-1.0	-0.7	-2.5	-1.7	-11.8	-7.8	-14.8	-10.5
Winter	Maximum (daytime)	-1.2	-0.8	-1.6	-0.9	-18.8	-14.8	-21.1	-16.9
	Maximum (nighttime)	-1.9	-1.3	-2.7	-2.1	-11.7	-8.5	-18.3	-13.4
	Daytime average	-0.8	-0.5	-1.3	-0.6	-13.4	-9.0	-15.8	-11.1
	Nighttime average	-1.4	-0.9	-1.9	-1.3	-8.6	-5.5	-14.3	-9.8
	Daily average	-1.1	-0.7	-1.6	-0.9	-11.2	-7.4	-15.1	-10.5

.

Table S9 | Seasonal impacts of PDRC-integrated RPVSP roofing configurations on building energy consumptions and RPVSP energy generation across Delhi and Kuala Lumpur. Relative changes in net building energy consumption (%) and RPVSP energy generation (%) are presented for summer and winter conditions with respect to the baseline RCC+RPVSP configuration. Corresponding absolute changes are provided in parentheses (W m^{-2}). Values represent spatial averages across urban grid cells. Negative values in building energy consumption indicate reduced cooling demand or enhanced energy savings, whereas positive values indicate increased heating demand during winter. Zero nighttime RPVSP generation reflects the absence of photovoltaic operation under non-solar conditions.

Seasons	Parameters	Building energy consumption		RPVSP energy generation	
		Delhi	Kuala Lumpur	Delhi	Kuala Lumpur
Summer	Maximum (daytime)	-13.9 (-3.5)	-12.1 (-2.6)	13.9 (3.5)	11.1 (2.4)
	Maximum (nighttime)	-22.7 (-5.4)	-19.8 (-4.0)	0.0	0.0
	Daytime average	-11.7 (-2.8)	-10.2 (-2.1)	9.6 (2.0)	7.8 (1.4)
	Nighttime average	-15.3 (-3.1)	-13.2 (-2.3)	0.0	0.0
	Daily average	-13.4 (-2.9)	-11.6 (-2.2)	5.2 (1.1)	4.2 (0.8)
Winter	Maximum (daytime)	3.6 (0.2)	2.9 (0.1)	15.7 (2.9)	12.9 (2.0)
	Maximum (nighttime)	5.9 (0.5)	4.8 (0.3)	0.0	0.0
	Daytime average	3.1 (0.1)	2.4 (0.1)	10.7 (1.7)	9.1 (1.2)
	Nighttime average	4.1 (0.3)	3.2 (0.2)	0.0	0.0
	Daily average	3.6 (0.2)	2.8 (0.1)	5.8 (0.9)	4.9 (0.6)

Table S10 | Configuration and physical parameterization schemes of the WRF–BEP+BEM modelling system employed in the present study.

Configuration	Domain 01 (d01)	Domain 02 (d02)	Domain 03 (d03)
Version	WRF-ARW model (v4.7.1)		
Initial and boundary conditions	NCEP GFS 0.25° x 0.25° (NCEP GFS 2015)		
Run time for Kolkata and Delhi (summer months)	31 March to 1 June 2025		
Run time for Kuala Lumpur (summer months)	31 May to 1 August 2025		
Analysis time for Kolkata and Delhi (summer months)	1 April to 31 May 2025		
Analysis time for Kuala Lumpur (summer months)	1 June to 31 July 2025		
Run time for Kolkata and Delhi (summer months)	30 November to 1 February 2026		
Run time for Kuala Lumpur (summer months)	31 August to 1 November 2025		
Analysis time for Kolkata and Delhi (winter months)	1 December to 28 February 2026		
Analysis time for Kuala Lumpur (winter months)	1 September to 31 October 2025		
Grid distance (km)	18	6	2
Grid number for Kolkata	75 x 75	91 x 91	121 x 121
Grid number for Delhi	100 x 100	88 x 88	76 x 76
Grid number for Kuala Lumpur	100 x 100	88 x 88	76 x 76
Number of vertical layers	40 layers		
Thickness of lowest model level	15 m		
Microphysics	WRF single-moment 6-class scheme (Hong et al., 2006)		
Surface layer model	Noah-LSM and BEP+ BEM (Chen ad Dudhia, 2001; Salamanca et al., 2010; Salamanca and Martilli, 2010; Martilli et al., 2002)		
Turbulence	TKE scheme (Janjic, 1994)		
Short-wave radiation	Dudhia scheme (Dudhia, 1989)		
Long-wave radiation	RRTM scheme (Mlawer et al.,1997)		
Planetary boundary layer	Bougeault-Lacarrere (BouLac) PBL scheme (Bougeault,and Lacarrere,1989).		
Cumulus parameterization	Kain-Fritsch (KF) scheme (Kain, 2004)		

Table S11 | Numerical design and optical parameterization of rooftop PDRC configurations integrated with RPVSPs used in the present study.

Scenarios	Types of roof surface	Optical properties of roof surface materials			Purpose
		Reflectance (ρ)	Emissivity (ε)	RPVSP fraction	
RCC+RPVSP	Conventional roof with urban photovoltaic	0.15	0.90	1.0	Baseline/Control
nm-PDRC+RPVSP	Standard PDRC roof with urban photovoltaic	0.95	0.93	1.0	Experimental
ρ-PDRC+RPVSP	Reflectance modulated PDRC roof with urban photovoltaic	0.15	0.93	1.0	Experimental
ε-PDRC+RPVSP	Emissivity modulated PDRC roof with urban photovoltaic	0.95	0.20	1.0	Experimental
ρε-PDRC+RPVSP	Combined reflectance and emissivity modulated PDRC roof with urban photovoltaic	0.15	0.15	1.0	Experimental
Current urban with RCC	Conventional roof	0.15	0.90	-	Model validation

Table S12 | Statistical evaluation of simulated 2-m air temperature ($T_{ambient}$) and 2-m relative humidity ($H_{relative}$) against observations across urban monitoring stations during the summer period over Kolkata.

Stations	2 m air temperature (°C)					2 m relative humidity (%)				
	r	MBE	MAE	RMSE	IOA	r	MBE	MAE	RMSE	IOA
Ballygunge	0.98	-0.35	0.99	1.02	0.97	0.99	-6.00	6.02	6.13	0.97
Belur Math	0.98	-0.10	0.83	0.89	0.98	0.98	-5.72	5.73	5.90	0.98
Bidhannagar	0.98	-0.06	0.90	0.94	0.98	0.97	-5.73	5.75	5.88	0.96
Jadavpur	0.97	-0.45	1.05	1.12	0.96	0.98	-6.34	6.38	6.68	0.97
Rabindra Bharati University	0.98	-0.16	0.85	0.88	0.98	0.96	-5.38	5.39	5.45	0.95
Rabindra Sarobar	0.96	-0.24	0.90	0.97	0.97	0.98	-5.99	5.98	6.12	0.96
Average	0.98	-0.23	0.92	0.97	0.97	0.97	-5.87	5.87	6.03	0.96

Table S13 | Statistical evaluation of simulated 2-m air temperature ($T_{ambient}$) and 2-m relative humidity ($H_{relative}$) against observations across urban monitoring stations during the winter period over Kolkata.

Stations	2 m air temperature (°C)					2 m relative humidity (%)				
	r	MBE	MAE	RMSE	IOA	r	MBE	MAE	RMSE	IOA
Ballygunge	0.98	0.87	0.88	0.89	0.98	0.99	-5.60	5.61	5.67	0.93
Belur Math	0.97	0.81	0.82	0.82	0.97	0.98	-6.21	6.22	6.25	0.88
Bidhannagar	0.98	0.94	0.94	0.95	0.95	0.98	-6.54	6.54	6.70	0.88
Jadavpur	0.98	0.98	0.97	0.99	0.95	0.98	-5.77	5.77	5.80	0.86
Rabindra Bharati University	0.96	1.11	1.12	1.12	0.96	0.96	-6.78	6.79	6.80	0.92
Rabindra Sarobar	0.98	0.71	0.70	0.72	0.97	0.96	-5.86	5.87	5.91	0.89
Average	0.98	0.90	0.91	0.92	0.96	0.98	-6.13	6.14	6.19	0.89

References

1. Atiganyanun, S., Plumley, J. B., Han, S. J., Hsu, K., Cytrynbaum, J., Peng, T. L., ... & Han, S. E. (2018). Effective radiative cooling by paint-format microsphere-based photonic random media. *Acs Photonics*, *5*(4), 1181-1187.
2. Cai, X., Wang, Y., Luo, Y., Xu, J., Zhao, L., Lin, Y., ... & Li, D. (2022). Rationally tuning phase separation in polymeric membranes toward optimized all-day passive radiative coolers. *ACS applied materials & interfaces*, *14*(23), 27222-27232.
3. Chae, D., Kim, M., Jung, P. H., Son, S., Seo, J., Liu, Y., ... & Lee, H. (2020). Spectrally selective inorganic-based multilayer emitter for daytime radiative cooling. *ACS applied materials & interfaces*, *12*(7), 8073-8081.
4. Chae, D., Son, S., Lim, H., Jung, P. H., Ha, J., & Lee, H. (2021). Scalable and paint-format microparticle–polymer composite enabling high-performance daytime radiative cooling. *Materials Today Physics*, *18*, 100389.
5. Gamage, S., Banerjee, D., Alam, M. M., Hallberg, T., Åkerlind, C., Sultana, A., ... & Jonsson, M. P. (2021). Reflective and transparent cellulose-based passive radiative coolers. *Cellulose*, *28*(14), 9383-9393.
6. Huang, J., Fan, D., & Li, Q. (2022). Structural rod-like particles for highly efficient radiative cooling. *Materials Today Energy*, *25*, 100955.
7. Leroy, A., Bhatia, B., Kelsall, C. C., Castillejo-Cuberos, A., Di Capua H, M., Zhao, L., ... & Wang, E. N. (2019). High-performance subambient radiative cooling enabled by optically selective and thermally insulating polyethylene aerogel. *Science advances*, *5*(10), eaat9480.
8. Li, T., Zhai, Y., He, S., Gan, W., Wei, Z., Heidarinejad, M., ... & Hu, L. (2019). A radiative cooling structural material. *Science*, *364*(6442), 760-763.
9. Li, N., Wang, J., Liu, D., Huang, X., Xu, Z., Zhang, C., ... & Zhong, M. (2019). Selective spectral optical properties and structure of aluminum phosphate for daytime passive radiative cooling application. *Solar Energy Materials and Solar Cells*, *194*, 103-110.
10. Li, X., Peoples, J., Huang, Z., Zhao, Z., Qiu, J., & Ruan, X. (2020). Full daytime sub-ambient radiative cooling with high figure of merit in commercial-like paints. *arXiv preprint arXiv:2008.03372*.
11. Li, X., Peoples, J., Yao, P., & Ruan, X. (2021). Ultrawhite BaSO4 paints and films for remarkable daytime subambient radiative cooling. *ACS applied materials & interfaces*, *13*(18), 21733-21739.
12. Li, J., Wang, X., Liang, D., Xu, N., Zhu, B., Li, W., ... & Zhu, J. (2022). A tandem radiative/evaporative cooler for weather-insensitive and high-performance daytime passive cooling. *Science Advances*, *8*(31), eabq0411.

13. Lin, C., Li, Y., Chi, C., Kwon, Y. S., Huang, J., Wu, Z., ... & Huang, B. (2022). A solution-processed inorganic emitter with high spectral selectivity for efficient subambient radiative cooling in hot humid climates. *Advanced Materials*, *34*(12), 2109350.
14. Liu, B. Y., Xue, C. H., Zhong, H. M., Guo, X. J., Wang, H. D., Li, H. G., ... & Wang, Z. (2021). Multi-bioinspired self-cleaning energy-free cooling coatings. *Journal of Materials Chemistry A*, *9*(43), 24276-24282.
15. Liu, R., Zhou, Z., Mo, X., Liu, P., Hu, B., Duan, J., & Zhou, J. (2022). Green-manufactured and recyclable coatings for subambient daytime radiative cooling. *ACS Applied Materials & Interfaces*, *14*(41), 46972-46979.
16. Mandal, J., Fu, Y., Overvig, A. C., Jia, M., Sun, K., Shi, N. N., ... & Yang, Y. (2018). Hierarchically porous polymer coatings for highly efficient passive daytime radiative cooling. *Science*, *362*(6412), 315-319.
17. Nie, X., Yoo, Y., Hewakuruppu, H., Sullivan, J., Krishna, A., & Lee, J. (2020). Cool white polymer coatings based on glass bubbles for buildings. *Scientific reports*, *10*(1), 6661.
18. Shi, M., Song, Z., Ni, J., Du, X., Cao, Y., Yang, Y., ... & Wang, J. (2023). Dual-mode porous polymeric films with coral-like hierarchical structure for all-day radiative cooling and heating. *Acs Nano*, *17*(3), 2029-2038.
19. Tsai, M. T., Chang, S. W., Chen, Y. J., Chen, H. L., Lan, P. H., Chen, D. C., ... & Wan, D. (2023). Scalable, flame-resistant, superhydrophobic ceramic metafibers for sustainable all-day radiative cooling. *Nano Today*, *48*, 101745.
20. Wang, X., Liu, X., Li, Z., Zhang, H., Yang, Z., Zhou, H., & Fan, T. (2020). Scalable flexible hybrid membranes with photonic structures for daytime radiative cooling. *Advanced Functional Materials*, *30*(5), 1907562.
21. Wang, T., Wu, Y., Shi, L., Hu, X., Chen, M., & Wu, L. (2021). A structural polymer for highly efficient all-day passive radiative cooling. *Nature communications*, *12*(1), 365.
22. Wang, X., Zhang, Q., Wang, S., Jin, C., Zhu, B., Su, Y., ... & Zhu, J. (2022). Sub-ambient full-color passive radiative cooling under sunlight based on efficient quantum-dot photoluminescence. *Science Bulletin*, *67*(18), 1874-1881.
23. Wu, X., Li, J., Xie, F., Wu, X. E., Zhao, S., Jiang, Q., ... & Zhang, R. (2024). A dual-selective thermal emitter with enhanced subambient radiative cooling performance. *Nature Communications*, *15*(1), 815.
24. Xiang, B., Zhang, R., Luo, Y., Zhang, S., Xu, L., Min, H., ... & Meng, X. (2021). 3D porous polymer film with designed pore architecture and auto-deposited SiO2 for highly efficient passive radiative cooling. *Nano Energy*, *81*, 105600.
25. Yue, Q., Zhang, L., He, C. Y., Liu, B. H., Wang, W. M., Lu, Z. W., ... & Gao, X. H. (2023). Polymer composites with hierarchical architecture and dielectric particles for efficient daytime subambient radiative cooling. *Journal of Materials Chemistry A*, *11*(6), 3126-3135.
26. Zhang, H., Ly, K. C., Liu, X., Chen, Z., Yan, M., Wu, Z., ... & Fan, T. (2020). Biologically inspired flexible photonic films for efficient passive radiative cooling. *Proceedings of the National Academy of Sciences*, *117*(26), 14657-14666.
27. Zhao, D., Aili, A., Zhai, Y., Lu, J., Kidd, D., Tan, G., ... & Yang, R. (2019). Subambient cooling of water: toward real-world applications of daytime radiative cooling. *Joule*, *3*(1), 111-123.
28. Zhao, H., Sun, Q., Zhou, J., Deng, X., & Cui, J. (2020). Switchable cavitation in silicone coatings for energy-saving cooling and heating. *Advanced Materials*, *32*(29), 2000870.
29. Zhong, H., Zhang, P., Li, Y., Yang, X., Zhao, Y., & Wang, Z. (2020). Highly solar-reflective structures for daytime radiative cooling under high humidity. *ACS Applied Materials & Interfaces*, *12*(46), 51409-51417.
30. Zhong, S., Yi, L., Zhang, J., Xu, T., Xu, L., Zhang, X., ... & Cai, Y. (2021). Self-cleaning and spectrally selective coating on cotton fabric for passive daytime radiative cooling. *Chemical Engineering Journal*, *407*, 127104.

31. Zhou, K., Li, W., Patel, B. B., Tao, R., Chang, Y., Fan, S., ... & Cai, L. (2021). Three-dimensional printable nanoporous polymer matrix composites for daytime radiative cooling. *Nano letters*, *21*(3), 1493-1499.
32. Zhu, Y., Ye, Y. H., Wang, D., & Cao, Y. (2021). Quasi-periodic selective multilayer emitter for sub-ambient daytime radiative cooling. *AIP Advances*, *11*(2).
33. Zhu, B., Li, W., Zhang, Q., Li, D., Liu, X., Wang, Y., ... & Zhu, J. (2021). Subambient daytime radiative cooling textile based on nanoprocessed silk. *Nature nanotechnology*, *16*(12), 1342-1348.